Accepted Manuscript

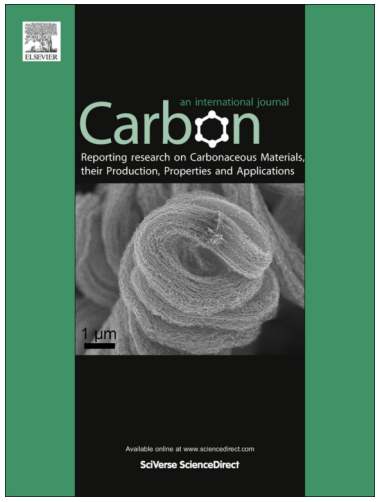

Electrochemically exfoliated graphene oxide/iron oxide composite foams for lithium storage, produced by simultaneous graphene reduction and $Fe(OH)_3$ condensation

Zhen Yuan Xia, Di Wei, Elzbieta Anitowska, Vittorio Bellani, Luca Ortolani, Vittorio Morandi, Massimo Gazzano, Alberto Zanelli, Stefano Borini, Vincenzo Palermo

PII: S0008-6223(14)01157-9
DOI: http://dx.doi.org/10.1016/j.carbon.2014.12.007
Reference: CARBON 9547

To appear in: *Carbon*

Received Date: 29 August 2014
Accepted Date: 1 December 2014

Please cite this article as: Xia, Z.Y., Wei, D., Anitowska, E., Bellani, V., Ortolani, L., Morandi, V., Gazzano, M., Zanelli, A., Borini, S., Palermo, V., Electrochemically exfoliated graphene oxide/iron oxide composite foams for lithium storage, produced by simultaneous graphene reduction and $Fe(OH)_3$ condensation, *Carbon* (2014), doi: http://dx.doi.org/10.1016/j.carbon.2014.12.007

Electrochemically exfoliated graphene oxide/iron oxide composite foams for lithium storage, produced by simultaneous graphene reduction and $Fe(OH)_3$ condensation

Zhen Yuan Xia [a], Di Wei [b], Elzbieta Anitowska [a], Vittorio Bellani [c], Luca Ortolani [d], Vittorio Morandi [d], Massimo Gazzano [a], Alberto Zanelli [a], Stefano Borini [b], Vincenzo Palermo [a*]

[a] *Istituto per la Sintesi Organica e la Fotoreattività - Consiglio Nazionale delle Ricerche, via Gobetti 101, 40129 Bologna, Italy*

[b] *Nokia R&D UK Ltd, Broers Building, 21 J. J. Thomson Avenue, CB3 0FA, Cambridge, UK.*

[c] *Dipartimento di Fisica and CNISM, Universitá degli Studi di Pavia, via Bassi 6, 27100 Pavia, Italy*

[d] *Istituto per la Microelettronica e Microsistemi - Consiglio Nazionale delle Ricerche, via Gobetti 101, 40129 Bologna, Italy*

Abstract

We describe the production of graphene-based composites for energy storage, obtained by a combination of electrochemical and solution processing techniques. Electrochemically exfoliated graphene oxide sheets (EGO) are produced using an original setup that allows fast expansion of graphite flakes and efficient exfoliation of expanded graphite *via* an electrochemical route. The sheets are deposited on a sacrificial nickel foam together with an iron hydroxide colloidal precursor. Calcination treatment simultaneously renders the EGO foam conductive and transforms $Fe(OH)_3$ into hematite (α-Fe_2O_3), yielding a nanoporous Fe_2O_3 layer on the surface of the mesoporous EGO foam, creating an ideal structure for lithium storage. The obtained graphene/metal oxide hybrid is a continuous, electrically conductive three-dimensional (3D) composite featuring a hierarchical meso-nano porous structure. A systematic study of these composites, varying the Fe_2O_3:EGO ratio, is then performed to maximize their performance as nanostructured electrodes in standard coin cell batteries.

* Corresponding author. E-mail: vincenzo.palermo@isof.cnr.it

1. Introduction

Lithium-based batteries are becoming increasingly popular for portable electronics applications, thanks to a growing demand for lightweight and flexible high-performance energy storage devices. A commonly used electrode is graphite, which has a limited theoretical capacity of 372 mA h g^{-1}.[1]. To meet the industrial demand for higher energy density batteries, alternative anode materials based on transition metal oxides have been used to improve the storage capacity of electrodes, due to their reversible conversion reactions with lithium (M_aX_b + ($b \cdot n$) Li ↔ aM + $b$$Li_nX$, where M = transition metal, X = anion, and n = formal oxidation state of X).[2] Among these metal oxides, Fe_2O_3 is a promising low-cost, abundant and non-toxic candidate for pseudo-capacitor electrodes with high theoretical capacity (1007 mA h g^{-1}, assuming ~6 Li per formula unit).[3] However, the practical applications of Fe_2O_3 based electrodes suffer from their low electrical conductivity and inferior cycling stability.[4]

Graphene, as a one-atom-thick layer of graphite, holds fascinating characteristics such as high surface area, excellent electrical conductivity, extraordinary elasticity and ultra-light weight. The integration of graphene sheets with metal oxides can efficiently enhance the electrical conductivity and improve the stability of these pseudo-capacitive materials.[5-9] Recently, three-dimensional (3D) graphene networks with porous architectures have been extensively investigated as excellent building blocks for electrochemically active metal particles. These freestanding 3D graphene-based foams (GF) couple a low density with the high flexibility and electrical conductivity of 2D graphene sheets. Meanwhile, the mesoporous or nanoporous[5, 10] morphology of GF gives a large contact area between the electrolyte and the electrode, and provides multidimensional electron transport pathways to enhance the electrochemical performance. The production of porous electrodes using 2D sheets thus seems a very promising approach for energy storage, as demonstrated by the large number of papers published recently on this field.[11-23] However, the starting material used to prepare these foams is usually graphene oxide (typically produced by Hummers method), that requires many days of preparation and tedious purification.[24] Alternatively, graphene can be grown directly on the metal substrate by chemical vapour deposition (CVD), but this approach requires harsh reaction conditions like high temperature (800°-1000°C) and ultra-high vacuum.

To meet the urgent requirement of large scale fabrication of graphene from cheap raw materials, an alternative approach intensively studied in the last few years is to exfoliate graphite using an electric bias. Massive conversion of bulk graphite into soluble sheets of

electrochemically exfoliated graphene oxide (EGO) can be obtained in a few minutes, compared to several tens of hours needed for chemical exfoliation of GO. [25, 26]

In particular, electrochemical exfoliation in aqueous solutions of inorganic salts can give a high yield of few-layers EGO (>85%, ≤ 3 layers), a reduced amount of oxidative damage and a large lateral size (>40 μm).[25] Furthermore, combining electrochemical exfoliation in acetonitrile and microwave-triggered expansion, we recently obtained ≈ 75% yield of graphite exfoliation, with monolayer yield >50%, and 72 % of the sheets being larger than 1 μm.[26]

The electrochemical exfoliation of graphite occurs so fast and efficiently because of the mechanical action due to gas production in the graphite bulk, which creates a pressure of several hundred bar, blister formation and delamination of graphene sheets.[27] However, the process can be used only with electrically continuous materials such as graphite rods or highly oriented pyrolitic graphite (HOPG), while the ideal starting material would be low-cost graphite powder, or microscopic graphite flakes. Furthermore, the electrochemical expansion is so fast and violent that large amounts of mesoscopic, unexfoliated graphite particles can be dispersed in solution, together with the monoatomic EGO sheets. These particles are no longer electrically connected to the working electrode, so do not exfoliate further.

In this work, we describe a new approach to exfoliate abundant and cheap graphite flakes with an electrochemical approach, with a high exfoliation yield (50 %) of non-monolithic EGO flakes.

To demonstrate a potential application of this method, the EGO sheets were deposited together with an $Fe(OH)_3$ precursor on a sacrificial metal template, and then thermally annealed to obtain monolithic, conductive Fe_2O_3/reduced graphene oxide (RGO) composite networks.[28, 29] The material obtained in this way was characterized by Scanning Electron Microscopy (SEM), Raman Spectroscopy, Energy dispersive X-ray spectroscopy (EDX), and used as an electrode in lithium batteries.

2. Experimental

Materials:

Graphite Flakes (+100 mesh series) were purchased from Aldrich. Sodium perchlorate (Sigma-Aldrich, 98 %) and sulphuric acid (Sigma-Aldrich, 95-97 %) were used as electrolytes; acetonitrile (Sigma-Aldrich, 99 %), *N, N*-Dimethylformamide (Sigma, 99 %) and Deionized (DI) water were used as solvents. A platinum foil (99.99 %) with the size of 5 mm × 10 mm × 0.1 mm was used as an anode connector. A platinum wire (99.99 %, 0.3 mm) was used as a counter electrode. Nickel foams (380 g m^{-2} in areal density and 1.5 mm in thickness,

compressed to 0.2 mm) were used as 3D templates for graphene coating. PMMA (950 K, 4 % in anisole), obtained from Micro Resist Technology GmbH., was used as a support polymer for Ni etching step. PTFE (47 mm, 0.2 μm) membrane filters (47 mm, 0.2 μm) were purchased from GVS.

Synthesis of graphene based compounds

Electrochemical preparation of EGO.

Graphite flakes (1 g) were put into a Nylon filter bag (200 mesh porosity, corresponding to a pore size of ≈ 75 μm), and inserted into a porous plastic tube to keep the whole material coherent. The flakes were compressed by pressing a plastic cap on the top of the tube (Figure 1). The plastic tube with filter mesh had a mechanical containment role, keeping the graphite flakes compressed inside the tube to ensure that they were all electrically connected to the metal electrode, and thus subject to exfoliation. This method allowed to perform electrochemical exfoliation on non-monolithic powder samples.

A Platinum foil was connected to graphite on the top of the tube through a slot of the plastic cap, to act as working electrode. A platinum wire outside the tube was used as a counter-electrode. The ionic solution was prepared dissolving 1.3 g of sodium perchlorate in 10 mL of acetonitrile (1 mol L^{-1}). Then, exfoliation was performed following an approach already described in previous work.[26] In brief, uncharged acetonitrile molecules were intercalated in graphite by electrochemical treatment, due to the synergistic action of perchlorate ions dissolved in the acetonitrile. Then, the CH_3CN molecules were decomposed with microwaves, causing gas production and rapid graphite exfoliation. This method uses the gas produced by the decomposition of acetonitrile molecules as a powerful blowing agent to foster graphite exfoliation in a few seconds.[26]

The first electrochemical intercalation/exfoliation stage was carried out for 30 min by applying a DC bias on the graphite electrode at a voltage of + 5 V. After reaction, the partially exfoliated graphite samples were washed with acetonitrile several times and blow-dried with dry nitrogen for 2 min.

A commercial microwave oven (Whirlpool JT379) with rotating tray was used for further expansion. The graphite samples were placed in a porcelain crucible (capacity 50 mL) and heated in the microwave oven for 30 s under 90 W. Then, the expanded foam-like graphite was compressed again to make the whole material coherent. The material was fixed a second time in a porous plastic tube, connected to a Pt foil and further exfoliated in 0.1 M H_2SO_4 solution as an anode at + 10 V for 2 hours. Then, the graphene sheets were collected by vacuum filtration onto a PTFE membrane and cleaned several times by repeated washing with

DI water. Afterwards, the exfoliated flakes were redispersed in DMF by sonication for 30 min (37 kHz, ≈100 W effective ultrasonic power, Model ELMA P70H Ultrasonic). The graphene oxide solution was centrifuged at 2000 rpm for 30 min to remove any re-aggregated particles.

Preparation of $Fe(OH)_3$ solution.

6.5 g of $FeCl_3$ was dissolved in 20 mL DI water (2 mol L^{-1}). 1 ml of the prepared solution was dropped into 100 mL of 1:1 boiling distilled water/ isopropyl alcohol (IPA). The solution was kept boiling for 2 hours to obtain $Fe(OH)_3$ solution. After centrifugation at 10000 rpm and repeated washing with water and IPA several times to remove the chloride ions, $Fe(OH)_3$ (10 mg mL^{-1}) was obtained and redispersed in 20 mL IPA.

Preparation of graphene foam (GF) and Fe_2O_3/GF.

EGO solutions (0.7 mg mL^{-1} in DMF) were deposited onto a Ni foam (10 mm x 5 mm x 0.2 mm) positioned on a hot-plate at 150 °C by drop casting method, and allowed to slowly infiltrate into the foam to give graphene oxide/Ni foam.

A freestanding foam (GF) was obtained by etching the Ni foam substrate. First, the foam was soaked in a poly(methylmethacrylate) (PMMA) solution (4% in anisole) and baked at 150 °C for 30 min, then GF/Ni foam was etched in 10% HCl solution for 24 h at 80 °C to fully dissolve the Ni metal. The PMMA support layer is important to prepare this free-standing GF; without PMMA support, GF broke down or collapsed during the HCl acid etching step. PMMA was removed by immersing the foam in hot acetone. Energy Dispersive X-ray spectroscopy (EDX) confirmed the complete removal of Ni after this treatment.

Fe_2O_3/EGO composites were prepared by drop-casting a dilute $Fe(OH)_3$ solution (1 mg mL^{-1} in IPA) onto a GF placed on a hot-plate at 100 °C. The ratio of $Fe(OH)_3$ and EGO could be changed by casting different amounts of $Fe(OH)_3$ solution.

The samples were heated at 400 °C for 2 hours to reduce the EGO, decompose the $Fe(OH)_3$ (if present) and obtain GF or Fe_2O_3/GF composites. A different weight ratio of Fe_2O_3:GF (from 1:5 to 5:1 with the fixed total amount of 3 mg) was obtained by coating different amounts of EGO and $Fe(OH)_3$, and measuring the weight difference after each coating. The weight loss measured for our EGO after heating was ≈30%. The weight loss from $Fe(OH)_3$ to Fe_2O_3 was around 27 %, which is consistent with the calculation ($2Fe(OH)_3 \rightarrow Fe_2O_3 + 3H_2O$, weight loss of water is 25.2 %). In all cases, the weight loss of EGO and $Fe(OH)_3$ was accounted for in the calculation to obtain the correct Fe_2O_3/GF ratio. This procedure was performed either on samples still having the underlying Nickel substrate, or on pure, freestanding GF.

Electrochemical Measurements and Characterization.

Cyclic voltammetry (CV) studies were carried out using a 1.0 mol L^{-1} Na_2SO_4 solution in ultra pure water (0.56 μS cm^{-1}) with an AMEL 5000 three electrode system setup. Foams partially immersed in the solution acted as the working electrode (only the immersed volume was used for calculations). The reference electrode was an aqueous Saturated Calomel Electrode (SCE), and the auxiliary electrode was a Pt wire separated from the working electrode by a glass frit. Specific capacitance values were calculated from the CV curves using the following equation: $C = (\int Idt)/(m\Delta V)$, where I is the oxidation or reduction current, dt is time differential, m is the mass of the active graphene foam, and ΔV is the voltage range of one sweep segment.

Standard 2032 coin cells were assembled inside a MBRAUN glovebox (H_2O< 2 ppm, O_2< 10 ppm) using GF or Fe_2O_3/GF samples with varying Fe_2O_3/GF ratios. In such a primary lithium battery, lithium foil is used as the anode with a polymer electrolyte composed of high molecular weight poly(ethylene glycol) borate ester. The Lewis acid centers of the borate esters interact with the anion resulting in enhanced lithium ion transport, and the resulting performance of such polymer electrolytes is comparable with conventional liquid organic electrolytes at room temperature. The prepared graphene foams were used directly as the cathode.

The electrical resistance of the graphene foams was measured with a four-point probe system (Keithley 2700 Multimeter). Scanning Electron Microscopy (SEM) images were obtained with a ZEISS 1530 instrument. Raman scattering measurements were carried out with a micro-Raman spectrometer (Model: LabRAM from Horiba Jobin-Yvon), using a 100 × objective (laser spot diameter ≈ 5 μm), laser excitation wavelength of 632.8 nm and laser power ~ 4 mW. XRD measurements were collected with a PANalytical X'PertPro instrument in Bragg-Brentano reflection mode (λ = 0.1542 nm, X'Celerator detector).

3. Results and Discussion

3.1 Morphology and structure

In this work we used cheap, natural graphite flakes as starting materials instead of the expensive, highly oriented pyrolytic graphite (HOPG) previously employed. After intercalation, expansion and exfoliation steps, EGO solutions were obtained with good yield (~35 %) and concentration (0.7 mg mL^{-1}). Moreover, the yield was further improved to 50 % by recycling the sediment and repeating the mild sonication/centrifugation step.

The high yield is due to the high density of material present and the confinement role of the polypropylene tube, which keeps the graphitic sheets associated even during electrochemical processing in sulphuric acids. The exfoliation of graphite anode at + 10 V promotes the intercalation of bisulphate ions into graphite, and the delamination of graphite inner layers due to gas evolution (O_2 and CO_2 from electrolysis of water and oxidation of graphite).[27] At the end of the process, we obtain a black-colored EGO slurry, which is solubilized very effectively by a mild sonication (30 min) in DMF with flakes spanning 1-10 um in length. A comparison of the sheets obtained by electrochemical exfoliation as compared to classical, extended sonication in DMF has been already reported in previous papers. [26, 27] Prolonged sonication in DMF yields non-defective graphene sheets [30], but sheet size is less than 1 um, and sonication time should be >400 hours to obtain high concentration. The approach described here gives sheets spanning 1-10 um in length, mostly mono- or bi-layers (for statistics see ref. [26, 27]), with concentration around 0.7 mg mL^{-1}.

The pre-expansion of graphite using acetonitrile and microwaves is fundamental to obtain a good yield.[26] After the rapid expansion process, the volume of graphite crystallites increased hundreds of times (see SEM images in Figure S1), which vastly facilitated the electrochemical intercalation of the bisulphate anion in the last step. Meanwhile, the mesoscopic Nylon mesh kept all the graphite electrically connected, and efficiently avoided the detachment of non-exfoliated flakes from the electrolysis of water and the following gas evolution.

By comparison, simple exfoliation of expanded graphite flakes with only a plastic tube and no Nylon filter produced exfoliated graphene with ~ 20 % yield due to the dispersion of flakes in the solution. After exfoliation and solubilization, the EGO sheets were deposited on a meso-porous nickel foam holder (~ 0.2 mm thick) acting as a sacrificial hard template.[11, 31] EGO solution was drop cast onto the foam, forming a continuous graphene layer on the nickel surface. After this, the Ni template could be removed by filling the foam with PMMA, etching the metal in acid, and removing the PMMA in a solvent. Figure 2 shows a schematic representation of the synthesis steps for this 3D structure.

A freestanding GF was obtained with size 20 mm x 10 mm x 0.2 mm, featuring low bulk resistance (22 Ω cm^{-2}) and areal density (≈ 1.0 mg cm^{-2}). This corresponds roughly to a volume density of ≈ 50 mg cm^{-3}, significantly greater than what is typically attainable with graphene foams grown by CVD on nickel templates (20 mg cm^{-3}, Ref. [12]).

The prepared free-standing GF forms an interconnected and monolithic 3D network structure (Figure 3). The weight of GF could be easily adjusted by varying the loading amount of EGO

solution on Ni. By using an EGO loading greater than 0.5 mg cm^{-2}, a continuous framework was formed, without the formation of cracks or collapse of the structure. A comparison of the GF before and after Ni etching is reported in Figure 3. The morphology with and without Ni is similar at both low and high magnification, confirming that the etching of the Ni template damages neither the foam nor the (possibly present) Fe_2O_3 coating. Few parts of the hollow internal branches are cracked, maybe due to escaped H_2 gas during the metal etching step ($2HCl + Ni \rightarrow NiCl_2 + H_2$). Besides this, the whole structure appears uniform and continuous, demonstrating the good coating properties of the EGO solution due to good affinity with the nickel surface.

To decorate the graphene network structure, a $Fe(OH)_3$ solution (3 mg mL^{-1}) was used as a precursor for α-Fe_2O_3 particles. A controlled amount of $Fe(OH)_3$ was drop cast onto the foam on a hot plate, then $Fe(OH)_3$ dehydration was induced simultaneously with reduction of EGO[32] by thermal annealing at 400 °C, much below the temperature required for graphene production by CVD (T=1000°C).[11]

The previously smooth graphene surface (Figure 4a,b) thus became uniformly covered by a porous Fe_2O_3 layer with pore sizes well below 100 nm (Figure 4c,d), formed during the condensation reaction at 400 °C and subsequent generation of vapour ($2\ Fe(OH)_3 \rightarrow Fe_2O_3 + 3\ H_2O$).

Figure 5 reports the Energy Dispersive X-ray spectroscopy (EDX) maps obtained on a segment of Fe_2O_3 /GF foam. Figure S2 in the Supporting Information shows the EDX spectrum from a small region on the foam. Both figures show clearly only the signal of carbon, oxygen, and iron, therefore confirming the complete removal of the nickel foam. Despite the low spatial resolution of the EDX maps (few μm), and the noise due the low acquisition time used to prevent sample damaging, the combination of EDX measurements and imaging shows that the nanoporous Fe_2O_3 layer is uniformly distributed on the GF foam (Figure 4 c,d).

The structure of the composite was characterized by X-ray diffraction (Figure 6) and Raman spectroscopy (Figure 7), given that both Fe_2O_3 and GF reveal a strong Raman signal and a typical XRD periodicity. Raman spectra of GF and Fe_2O_3/GF both showed the characteristic D peak (≈ 1329 cm^{-1}) and D' shoulder peak (≈ 1605 cm^{-1}) typical of GO and RGO, related to carbon defects in both spectra. [33] I_D/I_G ratio for GF and Fe_2O_3/GF were 0.5 and 1.4 respectively. The large, broad appearance of the D peak of the Fe_2O_3/GF sample is due to the contribution of the Fe_2O_3 two magnon scattering of hematite (≈ 1305 cm^{-1}), which also influence the different I_D/I_G ratio compared to the pure GF sample. The G peak (≈ 1572 cm^{-1}) and 2D peak (≈ 2650 cm^{-1}) are typically associated with graphitic carbon. In comparison, bare

Fe_2O_3 powder shows distinctive peaks (219 cm^{-1}, 285 cm^{-1}, 402 cm^{-1}) attributed to $2A_{1g}$ and $4E_g$ Raman modes for the hematite phase.[34] These bands were also clearly observed in Fe_2O_3/GF sample, confirming that the iron oxide formed has a hematite structure. The XRD patterns of Fe_2O_3 agree also with the rhombohedral phase of hematite (JCPDS No. 33-0664). An XRD peak at 26°, corresponding to a spacing of ≈ 3.4 Å, is observed for GF and for Fe_2O_3/GF, in good agreement with what was previously observed for EGO.[27] Noteworthily, the XRD diffraction peaks were relatively broad for Fe_2O_3/GF composites, indicating that the iron oxide particles are non-crystalline or sub nano-crystalline and that EGO sheets are poorly stacked, a favourable condition to enhance lithium intercalation. XRD peaks of nickel were not detected in either Fe_2O_3/GF or bare GF samples, confirming that the etching process successfully removed the nickel template.

3.2 Energy Storage Application

Thanks to the approach based entirely on solution processing, the Fe_2O_3:EGO w/w ratio could be easily tuned allowing optimization of the capacitance of the material. Using this approach, different weight ratios of Fe_2O_3:EGO (1:5, 1:2, 1:1, 2:1, 5:1 w/w with a fixed total amount of 3 mg) were loaded into the Ni foam by separately drop casting EGO and $Fe(OH)_3$ onto the Ni template. The electrochemical properties of Fe_2O_3/GF/Ni composite were measured with a three-electrode system in a 1 M Na_2SO_4 aqueous solution (Figure S3 in SI). The cyclic voltammetry (CV) profile of the GF/Ni foam sample at a scan rate from 5 to 200 mV s^{-1} suggests a typical electrical double layer behaviour at all sweeping rates. For comparison, simple GF/Ni and Fe_2O_3/Ni foams were prepared as control samples. The capacitor value of GF/Ni foam was 58 F g^{-1} at 5 mV s^{-1}. After the decoration of iron oxide nanoparticles, the current response increased at least twice even at the lowest Fe_2O_3:EGO ratio tested (1:5). The highest capacitance was obtained with a Fe_2O_3:EGO ratio 2:1, demonstrating that the meso-porous structure of graphene and the nanostructured iron oxide nanoparticles interact well to ensure a low resistance and short-range diffusion pathways for ions. Conversely, bare Fe_2O_3/Ni foam samples showed low initial capacitance that dropped significantly at high scan rates.

An Fe_2O_3/EGO ratio of 2:1 exhibited the highest specific capacity of 220 F/g at a scan rate of 5 mV s^{-1}. Further increase of the iron oxide up to 5:1 (Fe_2O_3:GF) gave worse specific capacitances, possibly due to the poorly conducting upper layer of iron oxide (Figure 8).

The Fe_2O_3/GF composite could be used in Li storage materials as the cathode without a Ni or Cu based current collector and without any polymer binder. The prepared foams were thus

used directly as the working electrode (cathode) to construct standard 2032 coin-cell batteries with the Li-foil as the counter electrode (anode) and poly(ethylene glycol) borate ester as polymer electrolyte.[35]

When the graphene foam (GF) was coated with Fe_2O_3 at=2:1 ratio, we typically observed two voltage plateaus during the first charge and discharge step (Figure 9). Li insertion into the Fe_2O_3 hematite nanostructure gave the voltage plateau at ~ 1.6 V during charging, while the stepwise reduction $Fe^{3+} \rightarrow Fe$ due to the lithiation process during the discharge stage gave the long plateau observed at ~ 0.8 V. This discharge plateau obtained with Fe_2O_3/GF is much higher than the voltage plateau of the cell made of GF (ca. 0.4 V), indicating that much more energy can be retained in the Fe_2O_3/GF composite. Use of Fe_2O_3/GF also improves the stability of the energy capacity in the cycling performance.

With the decoration of Fe_2O_3 nanoporous coatings, the initial discharge capacities could be enhanced from 508 to 701 mAh g^{-1}, a value comparable to commercially available batteries, and a higher energy capacity could be retained after the first discharge/charge cycle. The 3D graphene foam matrix worked as an efficient current collector to transfer sufficient electrons to the active metal oxide, without any electrochemically non-active polymeric binder or conducting additives. Noteworthy, the cycling capability of the Fe_2O_3:EGO electrodes was also significantly better than that of pure GF, even if a significant, irreversible capacity loss was observed after a few tens of cycles (Figure 9). This loss could be ascribed to the partial detachment of the Fe_2O_3 nanostructure during the lithiation and delithiation processes, and the formation of an electronically insulating solid electrolyte interface film on the Fe_2O_3/GF surface during cycling.[4, 36] SEM images comparing the quality of the coatings for all the different Fe_2O_3:EGO ratios tested are available in Figure S4. In all samples we observed the presence of a very rough and thick Fe_2O_3 layer, which tends to crack at large thicknesses. These materials should be further developed and optimized to improve the performance and cyclability; however, it should be noted that the approach described here has the additional benefit of using binder-free skeleton materials, differently from other commercial approaches.

4. Conclusions

In summary, we used a homemade setup to electrochemically exfoliate EGO sheets starting from graphite powders. The EGO sheets obtained in this way were highly soluble and processable, and could be processed together with an $Fe(OH)_3$ precursor to produce monolithic, freestanding, electrically conductive three-dimensional (3D) networks. The $Fe(OH)_3$/EGO blend was then transformed by thermal annealing into Fe_2O_3/RGO, which could

be effectively used as an electrode in batteries. Preparation of Fe_2O_3/RGO composites in this way helped to avoid traditional hydrothermal or solvothermal synthesis routes that usually require high pressures and long reaction times. Loading different amounts of the precursor solutions we could easily modulate the weight ratio between graphene foam and Fe_2O_3, and thus maximize their performance when used in Lithium batteries. Combining nanoscale characterization with tests in commercial coin cells, the best results were obtained for an Fe_2O_3:EGO ratio of 2:1, yielding a capacity of 701 mAh g^{-1}. Electron microscopy, X-ray diffraction and Raman spectroscopy of the Fe_2O_3 and EGO confirmed the 3D nano-crystalline structure of the network and the absence of contaminants coming from the metallic template or the exfoliation process. Overall, all the techniques described (exfoliation/filtration, infiltration, thermal treatments) are also suitable to produce samples larger than the 10x20 mm ones described herein, and thus may be easily up-scaled.

5. Acknowledgements

The research leading to these results has received funding from the European Union Seventh Framework Programme under grant agreement n°604391 Graphene Flagship and the EC Marie-Curie ITN-GENIUS (PITN-GA-2010-264694). The project UPGRADE acknowledges the financial support of the Future and Emerging Technologies (FET) programme within the Seventh Framework Programme for Research of the European Commission, under FET-Open grant number: 309056. We acknowledge the Operative Program FESR 2007-2013 of Regione Emilia-Romagna – Attività I.1.1.

REFERENCES

1. J.R. Dahn, T. Zheng, Y.H. Liu, and J.S. Xue. MECHANISMS FOR LITHIUM INSERTION IN CARBONACEOUS MATERIALS. Science; 1995; 270; 590.
2. J. Cabana, L. Monconduit, D. Larcher, and M.R. Palacin. Beyond Intercalation-Based Li-Ion Batteries: The State of the Art and Challenges of Electrode Materials Reacting Through Conversion Reactions. Advanced Materials; 2010; 22; E170.
3. J. Chen, L.N. Xu, W.Y. Li, and X.L. Gou. alpha-Fe2O3 nanotubes in gas sensor and lithium-ion battery applications. Advanced Materials; 2005; 17; 582.
4. Q.M. Su, D. Xie, J. Zhang, G.H. Du, and B.S. Xu. In Situ Transmission Electron Microscopy Observation of the Conversion Mechanism of Fe2O3/Graphene Anode during Lithiation-Delithiation Processes. Acs Nano; 2013; 7; 9115.
5. X.J. Zhu, Y.W. Zhu, S. Murali, M.D. Stollers, and R.S. Ruoff. Nanostructured Reduced Graphene Oxide/Fe2O3 Composite As a High-Performance Anode Material for Lithium Ion Batteries. Acs Nano; 2011; 5; 3333.
6. J.S. Luo, J.L. Liu, Z.Y. Zeng, C.F. Ng, L.J. Ma, H. Zhang, J.Y. Lin, Z.X. Shen, and H.J. Fan. Three-Dimensional Graphene Foam Supported Fe3O4 Lithium Battery Anodes with Long Cycle Life and High Rate Capability. Nano Letters; 2013; 13; 6136.
7. W. Wei, S.B. Yang, H.X. Zhou, I. Lieberwirth, X.L. Feng, and K. Mullen. 3D Graphene Foams Cross-linked with Pre-encapsulated Fe3O4 Nanospheres for Enhanced Lithium Storage. Advanced Materials; 2013; 25; 2909.
8. Y.X. Xu, Z.Y. Lin, X.Q. Huang, Y. Wang, Y. Huang, and X.F. Duan. Functionalized Graphene Hydrogel-Based High-Performance Supercapacitors. Advanced Materials; 2013; 25; 5779.
9. Y. Yang, X.J. Fan, G. Casillas, Z.W. Peng, G.D. Ruan, G. Wang, M.J. Yacaman, and J.M. Tour. Three-Dimensional Nanoporous Fe2O3/Fe3C-Graphene Heterogeneous Thin Films for Lithium-Ion Batteries. Acs Nano; 2014; 8; 3939.
10. X.C. Dong, Y.W. Ma, G.Y. Zhu, Y.X. Huang, J. Wang, M.B. Chan-Park, L.H. Wang, W. Huang, and P. Chen. Synthesis of graphene-carbon nanotube hybrid foam and its use as a novel three-dimensional electrode for electrochemical sensing. Journal of Materials Chemistry; 2012; 22; 17044.
11. Z.P. Chen, W.C. Ren, L.B. Gao, B.L. Liu, S.F. Pei, and H.M. Cheng. Three-dimensional flexible and conductive interconnected graphene networks grown by chemical vapour deposition. Nature Materials; 2011; 10; 424.
12. J.Y. Ji, L.L. Zhang, H.X. Ji, Y. Li, X. Zhao, X. Bai, X.B. Fan, F.B. Zhang, and R.S. Ruoff. Nanoporous Ni(OH) Thin Film on 3D Ultrathin-Graphite Foam for Asymmetric Supercapacitor. Acs Nano; 2013; 7; 6237.
13. Z.S. Wu, Y. Sun, Y.Z. Tan, S.B. Yang, X.L. Feng, and K. Mullen. Three-Dimensional Graphene-Based Macro- and Mesoporous Frameworks for High-Performance Electrochemical Capacitive Energy Storage. Journal of the American Chemical Society; 2012; 134; 19532.
14. B.G. Choi, M. Yang, W.H. Hong, J.W. Choi, and Y.S. Huh. 3D Macroporous Graphene Frameworks for Supercapacitors with High Energy and Power Densities. Acs Nano; 2012; 6; 4020.
15. H.P. Cong, X.C. Ren, P. Wang, and S.H. Yu. Macroscopic Multifunctional Graphene-Based Hydrogels and Aerogels by a Metal Ion Induced Self-Assembly Process. Acs Nano; 2012; 6; 2693.

16. Y.H. Xue, J. Liu, H. Chen, R.G. Wang, D.Q. Li, J. Qu, and L.M. Dai. Nitrogen-Doped Graphene Foams as Metal-Free Counter Electrodes in High-Performance Dye-Sensitized Solar Cells. Angewandte Chemie-International Edition; 2012; 51; 12124.
17. J. Chen, K.X. Sheng, P.H. Luo, C. Li, and G.Q. Shi. Graphene Hydrogels Deposited in Nickel Foams for High-Rate Electrochemical Capacitors. Advanced Materials; 2012; 24; 4569.
18. P.M. Sudeep, T.N. Narayanan, A. Ganesan, M.M. Shaijumon, H. Yang, S. Ozden, P.K. Patra, M. Pasquali, R. Vajtai, S. Ganguli, A.K. Roy, M.R. Anantharaman, and P.M. Ajayan. Covalently Interconnected Three-Dimensional Graphene Oxide Solids. Acs Nano; 2013; 7; 7034.
19. M. Mecklenburg, A. Schuchardt, Y.K. Mishra, S. Kaps, R. Adelung, A. Lotnyk, L. Kienle, and K. Schulte. Aerographite: Ultra Lightweight, Flexible Nanowall, Carbon Microtube Material with Outstanding Mechanical Performance. Advanced Materials; 2012; 24; 3486.
20. H. Hu, Z.B. Zhao, W.B. Wan, Y. Gogotsi, and J.S. Qiu. Ultralight and Highly Compressible Graphene Aerogels. Advanced Materials; 2013; 25; 2219.
21. H.Y. Sun, Z. Xu, and C. Gao. Multifunctional, Ultra-Flyweight, Synergistically Assembled Carbon Aerogels. Advanced Materials; 2013; 25; 2554.
22. X.H. Cao, Y.M. Shi, W.H. Shi, G. Lu, X. Huang, Q.Y. Yan, Q.C. Zhang, and H. Zhang. Preparation of Novel 3D Graphene Networks for Supercapacitor Applications. Small; 2011; 7; 3163.
23. X.H. Xia, J.P. Tu, Y.J. Mai, R. Chen, X.L. Wang, C.D. Gu, and X.B. Zhao. Graphene Sheet/Porous NiO Hybrid Film for Supercapacitor Applications. Chemistry-a European Journal; 2011; 17; 10898.
24. E. Treossi, M. Melucci, A. Liscio, M. Gazzano, P. Samorì, and V. Palermo. High-Contrast Visualization of Graphene Oxide on Dye-Sensitized Glass, Quartz, and Silicon by Fluorescence Quenching. Journal of the American Chemical Society; 2009; 131; 15576.
25. K. Parvez, Z.-S. Wu, R. Li, X. Liu, R. Graf, X. Feng, and K. Mullen. Exfoliation of Graphite into Graphene in Aqueous Solutions of Inorganic Salts. Journal of the American Chemical Society; 2014; 136; 6083.
26. Z.Y. Xia, G. Giambastiani, C. Christodoulou, M.V. Nardi, N. Koch, E. Treossi, V. Bellani, S. Pezzini, F. Corticelli, V. Morandi, A. Zanelli, and V. Palermo. Synergic Exfoliation of Graphene with Organic Molecules and Inorganic Ions for the Electrochemical Production of Flexible Electrodes. Chempluschem; 2014; 79; 439.
27. Z.Y. Xia, S. Pezzini, E. Treossi, G. Giambastiani, F. Corticelli, V. Morandi, A. Zanelli, V. Bellani, and V. Palermo. The Exfoliation of Graphene in Liquids by Electrochemical, Chemical, and Sonication-Assisted Techniques: A Nanoscale Study. Advanced Functional Materials; 2013; 23; 4684.
28. M. Du, C.H. Xu, J. Sun, and L. Gao. Synthesis of alpha-Fe2O3 nanoparticles from Fe(OH)(3) sol and their composite with reduced graphene oxide for lithium ion batteries. Journal of Materials Chemistry A; 2013; 1; 7154.
29. H.J. Song, X.H. Jia, N. Li, X.F. Yang, and H. Tang. Synthesis of alpha-Fe2O3 nanorod/graphene oxide composites and their tribological properties. Journal of Materials Chemistry; 2012; 22; 895.
30. U. Khan, A. O'Neill, M. Lotya, S. De, and J.N. Coleman. High-Concentration Solvent Exfoliation of Graphene. Small; 2010; 6; 864.
31. Y.M. He, W.J. Chen, X.D. Li, Z.X. Zhang, J.C. Fu, C.H. Zhao, and E.Q. Xie. Freestanding Three-Dimensional Graphene/MnO2 Composite Networks As Ultra light and Flexible Supercapacitor Electrodes. Acs Nano; 2013; 7; 174.
32. A. Liscio, G.P. Veronese, E. Treossi, F. Suriano, F. Rossella, V. Bellani, R. Rizzoli, P. Samori, and V. Palermo. Charge transport in graphene-polythiophene blends as studied

by Kelvin Probe Force Microscopy and transistor characterization. Journal of Materials Chemistry; 2011; 21; 2924.

33. A.C. Ferrari and D.M. Basko. Raman spectroscopy as a versatile tool for studying the properties of graphene. Nature Nanotechnology; 2013; 8; 235.
34. S. Bai, S.Q. Chen, X.P. Shen, G.X. Zhu, and G.X. Wang. Nanocomposites of hematite (alpha-Fe2O3) nanospindles with crumpled reduced graphene oxide nanosheets as high-performance anode material for lithium-ion batteries. Rsc Advances; 2012; 2; 10977.
35. Y. Kato, K. Hasumi, S. Yokoyama, T. Yabe, H. Ikuta, Y. Uchimoto, and M. Wakihara. Polymer electrolyte plasticized with PEG-borate ester having high ionic conductivity and thermal stability. Solid State Ionics; 2002; 150; 355.
36. D. Larcher, C. Masquelier, D. Bonnin, Y. Chabre, V. Masson, J.B. Leriche, and J.M. Tarascon. Effect of particle size on lithium intercalation into alpha-Fe2O3. Journal of the Electrochemical Society; 2003; 150; A133.

FIGURE CAPTIONS

Figure 1. a) Schematic illustration of EGO preparation by electrochemical processing. b) Photograph of the EGO solution. In the inset, a representative AFM image of EGO flakes spin-coated on a SiO_x/Si substrate (Z-range: 20 nm). c) Photograph comparing the original Ni foam, the GF and the Fe_2O_3/GF samples.

Figure 2. Schematic illustration of GF and Fe_2O_3/GF synthesis routes.

Figure 3. SEM images of: a) Pristine Nickel foam. b) GF, c) Fe_2O_3/GF/Ni foam and d) Fe_2O_3/GF. Arrows in b) indicate rare cracks due to the etching of the nickel substrate.

Figure 4. SEM images of: a) GF, and c) Fe_2O_3/GF, 1:2 weight ratio. b,d) are zoom-in of a) and c) respectively. e) Cartoon showing the hierarchical structure of the Fe_2O_3/GF porous layer.

Figure 5. SEM image and EDX mapping of C, O, Fe elements on a segment of Fe_2O_3/GF foam.

Figure 6. XRD signal of Fe_2O_3 powder, GF and Fe_2O_3/GF.

Figure 7. Raman spectra of Fe_2O_3 powder, GF and Fe_2O_3/GF.

Figure 8. a) Comparison of specific capacitance values from the different materials tested. b) Specific capacitance values at the scan rate of 5 mV/s obtained for GF, Fe_2O_3 and for different composites with varying Fe_2O_3:GF ratio.

Figure 9. Electrochemical performance of GF and Fe_2O_3/GF 2:1 composite in coin-cell batteries, a) first-cycle discharge (lithium insertion) and charge (lithium extraction) curves of the products. b) Cycling performances of the products at the current density of 50 mA/g.